JOURNAL OF SPACECRAFT AND ROCKETS
Vol. 45, No. 5, September–October 2008

New Method to Predict Nonlinear Roll Damping Moments

F. G. Moore* and L. Y. Moore†
Aeroprediction, Inc., King George, Virginia 22485

DOI: 10.2514/1.34974

A new method was developed to approximate roll damping moments as a function of both Mach number and angle of attack. The method is applicable over the Mach number (0 to 20) and angle-of-attack (0–90-deg) ranges that the Aeroprediction code is applicable. The method attempts to account for the physical phenomena of wing load due to roll, wing aspect-ratio and stall effects, canard-shed vortices, fins on a boat tail or a flare, and body compressibility and viscous effects. The method does not account for the physical phenomena of nonlinear rolling moment due to high spin rate or asymmetric shedding of the body vortices. Both nonlinearities due to spin rate and asymmetric vortices appear to be significant at Mach numbers below 1.5 and angles of attack greater than about 20 deg. Comparison of the new method with existing experimental databases was very encouraging. However, additional data on various configurations (particularly wing–body–tail cases) are needed for further validation and refinement of the semi-empirical model.

Nomenclature

A_{ref}	=	reference area (maximum cross-sectional area of the body, with the body present, or of the planform area of the wing, with the wing alone), ft^2
A_W	=	wing planform area, ft^2
AR	=	aspect ratio
b	=	wing span (not including body), ft
C_ℓ	=	roll moment coefficient
C_{ℓ_p}	=	roll damping moment coefficient $[\gamma C_\ell/\gamma(pd/2V_\infty)]$
C_{ℓ_δ}	=	roll driving moment coefficient $(\gamma C_\ell/\gamma\delta)$
C_N	=	normal force coefficient
C_{N_B}	=	normal force coefficient of the body alone
C_{N_L}, $C_{N_{\text{NL}}}$	=	linear and nonlinear components of normal force coefficient
$C_{N_{T(V)}}$	=	normal force coefficient on tail as a result of wing-shed vortices
C_{N_W}	=	normal force coefficient of the wing alone
$C_{N_{W(B)}}$, $C_{N_{T(B)}}$	=	normal force coefficient of the wing or tail in the presence of the body
C_{N_α}, C_{N_δ}	=	normal force coefficient derivative (per radian) due to angle of attack or control deflection
C_P	=	pressure coefficient $(P - P_\infty)/\frac{1}{2}\rho_\infty V_\infty^2$
c, c_r, c_t	=	local chord, root, and tip chord, ft
d_{ref}	=	reference body diameter, ft
ℓ, ℓ_n, ℓ_a, ℓ_B	=	total body, nose, afterbody, or boat-tail length, ft or cal
M_N	=	Mach number normal to body $(M_\infty \sin\alpha)$
M_∞	=	freestream Mach number
MFF	=	multifin factor
NC	=	number of canards
P_L, P_∞	=	local and freestream pressure, lb/ft^2
p	=	roll rate, rad/s
Q_L, Q_∞	=	local or freestream dynamic pressure, lb/ft^2
r	=	local body radius
s	=	$r + b/2$
T_L, T_∞	=	local and freestream temperature, °R
V_∞, V_L	=	freestream and local velocity, ft/s
x, y, z	=	coordinate system, x along the body axis, y out of the right wing, and z up
y_c	=	distance from the body centerline to the wing centroid of the presented area
α	=	angle of attack, deg
$\Delta C_{N_{B(W)}}$, $\Delta C_{N_{B(T)}}$	=	additional normal force coefficient on the body in the presence of the wing or tail
θ_b, θ_f	=	boat-tail or flare angle, deg
ρ_∞	=	freestream density, slugs/ft^3
Φ	=	roll-position of missile fins (0 deg corresponds to fins in the plus orientation and 45 deg corresponds to fins rolled to the cross orientation)

Presented as Paper 4376 at the 38th AIAA Fluid Dynamics Conference, Seattle, WA, 20–25 June 2008; received 4 October 2007; revision received 21 March 2008; accepted for publication 31 March 2008.

*President; drfgmoore@hotmail.com. Associate Fellow AIAA.
†Computer Scientist.

Introduction

ROLL damping moment prediction in the Aeroprediction code, like pitch damping moments, had remained basically the same since the 1977 version of the code, the AP77 [1], was introduced. However, with the attention given to cheaper unguided weapons in the last 10 years, renewed interest has been placed on roll damping. The original AP77 developed an approximate method to calculate roll damping based on three-dimensional thin-wing theory supersonically [2,3] and lifting-surface theory subsonically [4]. For roll damping, the lifting surfaces were assumed to extend all the way to the body centerline and the r/s effect of the fins as well as the number of fins were accounted for by slender-body theory (see [5], p. 43). The body roll damping, which is basically negligible compared with the fins, was estimated empirically [6].

The improvements discussed in [7] add significant improvement to the near-zero angle-of-attack (AOA) prediction of roll damping moments when the configuration has a long boat tail. For many of the unguided weapons, they can experience high AOA due to launch conditions and, in some cases, due to low static margins. A combination of events can lead to reduced accuracy and, in the worst-case scenario, instability. It is therefore important to be able to predict roll damping at AOA to understand the flight performance of primarily unguided fin-stabilized weapons and, to a lesser extent, guided weapons near launch.

A literature survey was conducted for nonlinear roll damping and the references found will be broken down into experimental and theoretical categories. References [8–21] are the experimental references found for the nonlinear roll damping. References [22–25] are nonlinear theoretical models, and [26–30] are linear theoretical or

experimental data reports of interest. References [8,15] give experimental values of roll damping to high AOA for the Army–Navy finner (ANF) and a modified version of the ANF (MANF). Roll damping of the ANF was given for Mach numbers of 0.22 and 2.5 and for the MANF at Mach numbers of 0.6, 0.9, 1.15, 1.3, 1.5, 1.76, 2.0, and 2.5. The roll damping measurements were made using a base sting as opposed to a leeward plane strut mount as done for pitch damping. Hence, not as much interference from the sting onto the model should be present as for the pitch damping measurements.

Reference [11] complements [8,15] in that it gives roll damping results for the ANF determined earlier (1964) from the U.S. Naval Ordnance Laboratory Tunnel. Roll damping data are given at $M_\infty = 0.22$ for α of -10 to $+60$ deg, at $M_\infty = 0.77$ for α of -10 to $+10$ deg, at $M = 2.54$ for α of -10 to $+26$ deg, and at $M_\infty = 4.1$ for α of 0 to 22 deg. It is safe to say the ANF and MANF configurations have the most extensive roll damping database available when one combines [11,15].

Reference [9] gives the roll damping measurements for the 81-mm Australian mortar at $M_\infty = 0.5$ to 0.95 at $\alpha = 0$, 5, and 10 deg. However, the report notes the $M = 0.9$ and 0.95 results are questionable due to wind-tunnel transonic wall effects.

Reference [10] summarizes the Navy investigations up through 1959 of the Mark (MK) 82 low-drag bomb. Roll damping data of [10] include a Mach number of 0.8 at $\alpha = 0$–35 **deg** and Mach numbers 0.6–1.4 at $\alpha = 0$ **deg**. Reference [16] presents a complimentary set of data for the fixed-fin and inflatable stabilizer/retarder candidates for the MK 82 low-drag bomb. Roll damping results are given for Mach numbers 0.4–1.3 at $\alpha = 0$, 10, and 20 deg.

References [17,18] give component buildup roll damping data for a canard-control missile at $M_\infty = 0.1$ and $\alpha = 0$–30 deg. Several points are noteworthy in these two references. First, [17] showed roll damping for body–canard, body–tail, and canard–body–tail with and without control deflection. Results indicate the canard-shed vortices almost eliminate the roll damping of the tail surfaces. The second point of note was that the roll damping measurements for the canard–body–tail configuration of [17,18] agree up to α of 25 deg but, whereas [17] shows C_{ℓ_p} continuing its negative magnitude increase at $\alpha = 30$ deg, [18] showed C_{ℓ_p} approaching zero at $\alpha = 30$ deg. No explanation was given for the large divergence in C_{ℓ_p} at $\alpha = 30$ deg between the two references.

The remaining nonlinear data sets are unclassified but have limited distribution. Hence, one can discuss these data but cannot show the specific data or configuration without approval from the source. Reference [12] gives wind-tunnel measurements of the 2.75 wraparound fin rocket at $M_\infty = 4.25$ and $\alpha = 0$–10 deg. Instead of C_{ℓ_p} increasing in magnitude with AOA as would be expected, this report shows a decrease. It is not clear why, leading one to feel suspect of the results. Reference [19] gives results of a folding-fin 2.75-in.-diam rocket at Mach numbers of 2.5 to 4.5 for α of -5 to $+5$ deg. Roll damping trends increase in magnitude with AOA, as would be expected for these high Mach numbers. References [20,21] give the transonic and supersonic wind-tunnel test results of several axisymmetric bomblet munition models. Roll damping results are given for Mach numbers of 0.4 to 2.5 and for α of 0 to 11 deg. Results follow the trends that one would expect. One nice thing about the results of the [20,21] is that test data is available for very-low-aspect-ratio 6-fin configurations. The final two limited-distribution nonlinear roll damping data reports [13,14] are for mortar configurations in which the Mach number varies from 0.5 to 1.05 and α varies from 0 to 14 deg.

To summarize the nonlinear roll damping data available, it is fair to say that only two configurations (ANF and MANF) have a fairly extensive database available. Portions of other databases are available, but quite limited. What is needed is a component database similar to [17,18] that extend the aspect ratio of the wings, along with Mach number and AOA range. Not having such a database will hamper a semi-empirical model development and hinder the accuracy of any model developed. However, a nonlinear semi-empirical model for roll damping prediction is a goal of this work. The model can be refined and improved upon as more data become available.

The available nonlinear theoretical approaches for roll damping are even more limited than the experimental databases. Reference [22] gave a revised equation for roll, which includes not only C_{ℓ_δ} and C_{ℓ_p}, but C_ℓ as well. Also, the equation is a function of roll orientation and AOA. Unfortunately, the new nonlinear roll equation is of no value to predict nonlinear roll damping.

References [23,24] appear to be the most rigorous attempt to define nonlinear roll damping moments found in the literature. Oberkampf [23,24] made several fairly significant assumptions in his theoretical development, however. The assumptions include no effect of the fin on the body and a simplified lifting theory for the wing-alone solution, as opposed to a more rigorous lifting-surface or three-dimensional thin-wing-theory approach. On the other hand, Oberkampf's method made an assumption for boundary-layer separation that allowed him to bring into play the viscous effects at AOA and roll (because local AOA on a wing is a function of both α and Φ). References [23,24] showed reasonable comparisons of theory and experiment to the ANF and several other configurations at a limited set of conditions.

The last nonlinear method is given in [25]. The theory is compared with experiment on a couple of examples [25] with reasonable success; however, the theory is not defined in the reference, and so it is assumed that the [25] theory is not available in the open literature.

Before leaving the literature survey on nonlinear roll damping, several references for 0-deg-AOA roll damping are worthy of note. First is the Nicolaides and Bolz [26] method to compute low-AOA roll damping. The most interesting point about [26] was not the theoretical method, but they showed a component buildup of roll damping on the ANF with body–tail, body–wing (same size wing and tail), and body–wing–tail. Reference [26] indicated that at $M = 1.95$, the tail surfaces were only 14% as effective in roll damping in the wing–body–tail arrangement as in the body–tail configuration. At $M = 1.73$, no tail roll damping effectiveness was shown in the wing–body–tail arrangement. Hence, [27], like [17], showed a large loss in roll damping of the tail surfaces due to wing- or canard-shed vortices.

Reference [27] gave roll damping flight-test results of a wing–body–tail configuration similar to the Seasparrow missile. In using the AP05 code to compare theory with measurements, it is clear that there was a large loss in roll damping due to wing-shed vortices. Reference [27] also indicated a substantial loss in roll damping due to aeroelastic effects.

Prakash and Khurana [28] derived a simple approach to predict C_{ℓ_p} based on linearized wing theory and incorporation of wing–body and body–wing interference effects. They showed slightly improved results compared with Oberkampf [23] at supersonic speeds, but results were much too high subsonically. The AP77 [1] results were the best overall of all the theories presented in [28].

Eastman [29] showed that roll damping moment could be correlated quite well to roll driving moment for cruciform missiles. His formulation gave

$$C_{\ell_p} = -2.15(\bar{y}/d)C_{\ell_\delta} \tag{1}$$

where $\bar{y}$ is the radial distance from the body centerline to the exposed wing centroid. Examples of several configurations in which C_{ℓ_δ} were known were shown to compare well with the simple correlation equation (1). Mikhail [30] then extended Eastman's [29] theory to multiple fins that could be planar, wraparound, or offset from the body centerline.

To summarize the literature review of experimental data and analytical approaches for nonlinear roll damping, it is fair to say that the databases are very limited and the theoretical methods are even more limited. There was no robust theoretical method at all that could handle wing–body–tail configurations, which is the goal of the present work.

Nonlinear Roll Damping Model

Before we discuss analytical approaches to model nonlinear roll damping, it is appropriate to discuss some of the physical phenomena

that we will attempt to model in an approximate sense. The physics are dependent on Mach number, AOA, roll rate, and configuration geometry. Figures 1 and 2 attempt to illustrate some of the physical phenomena that occur when a missile rolls. For supersonic flow, shocks occur both on the nose of the body and on the leading edges of the canards and wings. Under certain conditions, these shocks may intersect a lifting surface, creating significant nonlinearities. In addition to the body vortices, each canard sheds a vortex at about 80% of the span. This vortex path will be slightly curved due to the roll and will intersect the tail surface(s). Typically, the intersection will occur on the outer part of the tail, where the load on the tail due to roll (see Fig. 1b) is the highest, thus having the largest impact on the roll damping of the tail, because the vortex lift is always opposite the wing lift. Also, for lift, only two wing-shed vortices need to be considered in the roll position $\Phi = 0$ deg, whereas for roll, all vortices from the forward lifting surfaces can adversely impact the roll damping of the tail surfaces.

Another physical phenomena that occurs from subsonic to low supersonic speeds is asymmetric shedding of vortices. This phenomena typically starts around $\alpha = 25$ deg, reaches a maximum around $\alpha = 45$ deg, and then goes to zero around $\alpha = 65$ deg. Although not mentioned in [17,18] as to why C_{ℓ_p} was so different at $\alpha = 30$ deg between the two identical tests, the fact that the results were identical at $\alpha = 25$ deg makes one suspicious of the asymmetric body-shed vortex as a possible source of the large difference in C_{ℓ_p}. Reference [8] also showed a strong nonlinearity in roll moments with roll rate at angles of attack greater than 20 deg and for Mach numbers less than 1.5 (particularly for Mach numbers 0.9 and lower). Fortunately, the Mach number and angle-of-attack range where the roll rate nonlinearities occur agrees very closely with the angle-of-attack and Mach number ranges in which asymmetric shedding of vortices occur. Hence, it is fair to say that the physics of nonlinear roll moment due to roll rate or asymmetric shedding of vortices will not be attempted in the present nonlinear roll damping moment. The implication of not including these two physical phenomena is that the nonlinear roll damping results will be questionable for AOA greater than 20 deg for Mach numbers less than 1.5 (particularly for Mach numbers less than 0.9).

Wing stall is also a physical phenomena that affects C_{ℓ_p}, particularly at subsonic Mach numbers. Wing stall is a function of the wing aspect ratio (see Fig. 2), Mach number, and AOA. For a high aspect ratio ($AR \geq 2.0$), wing stall typically occurs at $\alpha = 10$–15 deg at subsonic Mach numbers, whereas for a low aspect ratio ($AR \leq 0.5$), wing stall is hardly noticeable at any AOA. Moderate-aspect-ratio wings lie between the low- and high-aspect-ratio extremes. At high Mach numbers ($M > 2.0$), stall on wings is not nearly as noticeable, due to the high dynamic pressures in the windward plane dominating the flowfield.

Another physical phenomena for wing–body–tail configurations is the fact that all forward lifting surfaces will shed vortices when rolling, and these vortices will all adversely impact the roll damping effectiveness of the tail surfaces. As AOA increases, the impact of the forward shed vortices will diminish and the effectiveness of the tail surfaces on roll damping will improve.

Dynamic pressure (see Fig. 2) plays a significant role in roll damping effectiveness. At low AOA, all tail fins are effective in providing roll damping, whereas as AOA increases, the fins in the windward plane become more effective and the fins in the leeward plane become less effective at providing roll damping. At lower Mach numbers, where dynamic pressure is the lowest, the roll damping can actually decrease with AOA (particularly for higher-aspect-ratio fins), whereas at higher Mach numbers, the windward plane fins tend to dominate and hence the roll damping generally increases with increasing AOA. If the fins are located on a boat tail or flare, roll damping typically will decrease or increase, respectively, due to the lower or higher dynamic pressure on the boat tail or flare. Boat-tail effects were accounted for in [7], but the effects of a fin located on a flare must be considered in any new methodology. The physical phenomena that must be accounted for in a nonlinear model for roll damping prediction are as follows: asymmetric body-shed vortices ($25\,\text{deg} < \alpha < 65\,\text{deg}$ and $M_\infty < 2.0$), nonlinear roll moment due to high spin ($20\,\text{deg} < \alpha$ and $M_\infty \leq 1.5$), C_{N_α} of wing (AR and M_∞) and stall, angle of attack and dynamic pressure (all fins effective at $\alpha = 0$ and windward plane fins at moderate-to-high α), canard-shed vortices (all forward fins shed vortices in roll and impact on tail surfaces at the point of maximum normal force due to roll), and fins on a boat tail or flare.

As already mentioned, no attempt will be made to model the nonlinearities due to high roll rate or asymmetric body vortices. As a result, the accuracy of any new method will be questionable at AOA greater than about 20 deg and Mach numbers less than 1.5 (particularly for Mach numbers less than 0.9).

One now must translate the physical phenomena into a mathematical model that, it is hoped, will approximate roll damping

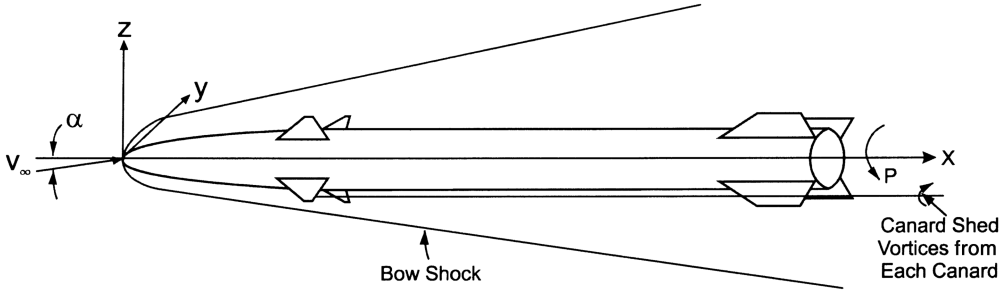

a) Rolling cruciform canard–body–tail configuration at supersonic Mach number

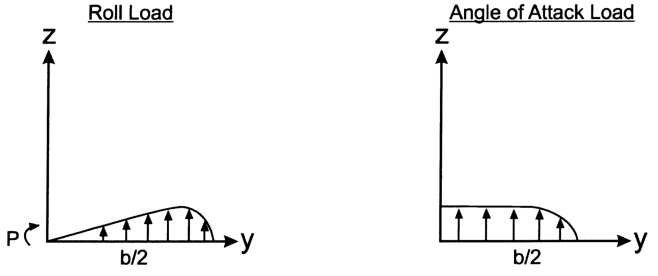

b) Wing load due to roll and angle-of-attack

Fig. 1 Some of the physical phenomena that occur on a rolling missile.

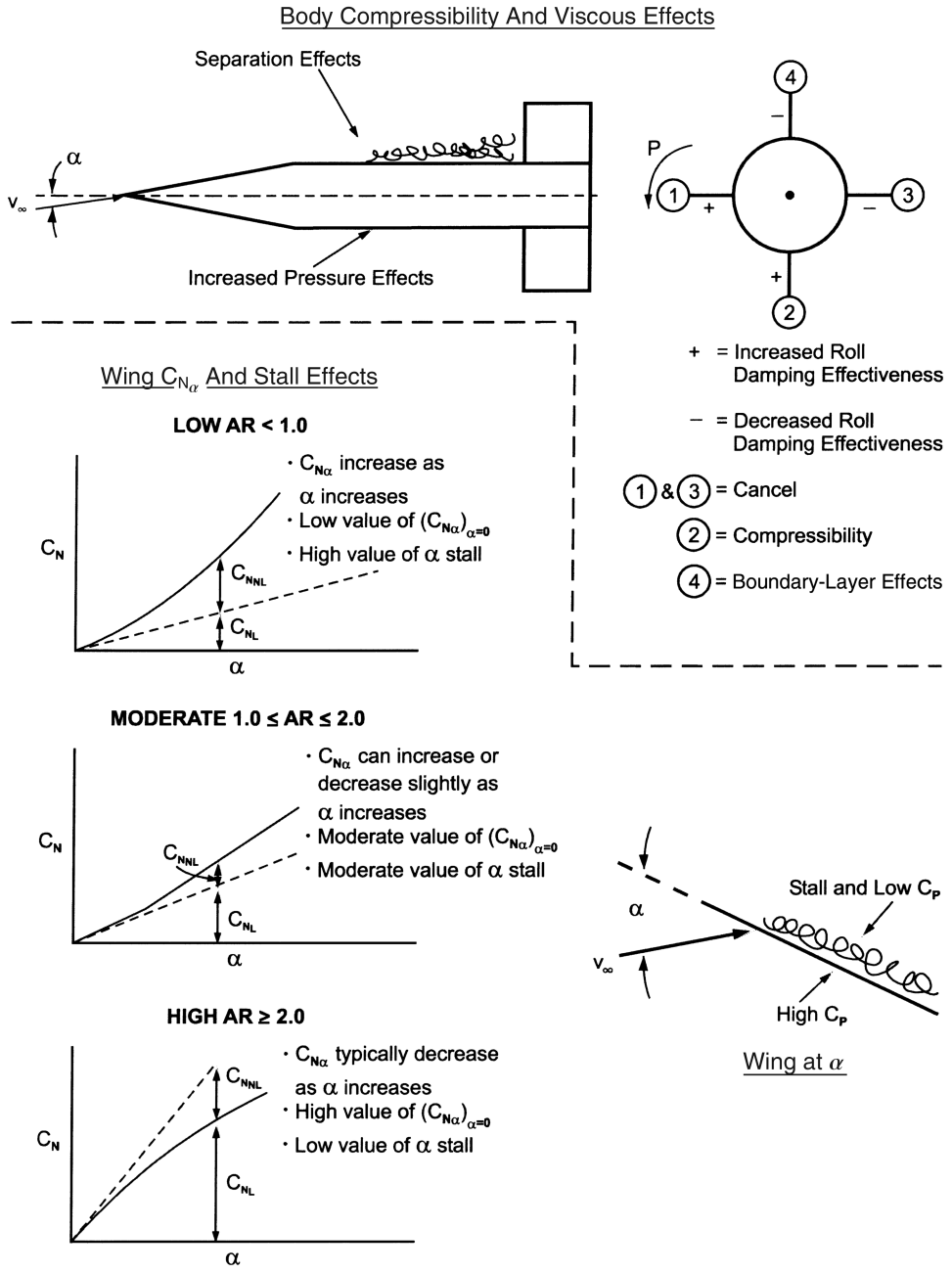

Fig. 2 Some of the physical phenomena affecting roll damping.

in a robust sense for weapon configurations. The improvements discussed in [7] should allow reasonable accuracy for roll damping of the body–tail configurations near $\alpha = 0$. However, an account of the adverse effect of canard- and wing-shed vortices on the tail surfaces has not been attempted nor have AOA or flare effects been accounted for. Thus, the goal will be to extend the accurate 0-deg-AOA roll damping prediction capability [7] to missiles with two sets of lifting surfaces and to weapons at non-0-deg AOA.

The first problem to be dealt with is the canard-shed vortices. There are three sets of data [17,26,27] that have roll damping at a 0-deg AOA for configurations with two sets of lifting surfaces. Moreover, two of the data sets [17,26] have component buildup data for roll damping that clearly shows the loss of tail effectiveness for roll damping when the forward lifting surfaces are placed on the wind-tunnel model. The approach taken here to model the loss of roll damping on the tail surfaces due to wings or canards is to use the comparison with the loss of lift on the tail surfaces due to the wings or canards. However, the effect on the tail surfaces needs to be doubled to account for the fact that all forward lifting surfaces impact the tail surfaces in roll, not just the surfaces that are affected by the flow normal to the body as is the case in calculating normal force. Also, a factor needs to be applied to the wing-shed vortex effect on the roll damping of the tail fins to account for the fact that the vortices intersect the tail fin, where the load due to roll is highest (see Fig. 1b). A model that appears to account for the loss of roll damping on the tail fins due to wing- and canard-shed vortices is

$$(C_{\ell_P})_{\mathrm{TM}} = (C_{\ell_P})_{\mathrm{TU}}\left[\frac{C_{N_{T(B)}} + \Delta C_{N_{B(T)}} + (\mathrm{NC})C_{N_{T(V)}}}{C_{N_{T(B)}} + \Delta C_{N_{B(T)}}}\right] \qquad (2)$$

where subscripts TM and TU stand for tail modified and tail unmodified, respectively.

Several points are worthy of note in Eq. (2). All the normal force terms in Eq. (2) contain all the nonlinearities in AOA, Mach number, and configuration geometry at both $\Phi = 0$ and 45 deg. $C_{N_{T(V)}}$ thus already contains canard/wing size and location in the calculation of downwash for both roll angles of 0 and 45 deg. The number of canards (NC) that multiples $C_{N_{T(V)}}$ accounts for four shed vortices impacting the tail versus two for the $C_{N_{T(V)}}$, along with an additional

factor of 2 for the vortex impacting the tail at the largest load due to roll. If the canards or wings are not cruciform, then NC is replaced by the number of canards or wings present. Finally, a constraint is placed on the factor in Eq. (2) that multiplies $(C_{\ell_P})_{\mathrm{TU}}$ that does not allow the factor to go negative, creating a positive roll damping of the tail fins. Of course, if there are no canards or wings present, the factor multiplying $(C_{\ell_P})_{\mathrm{TU}}$ in Eq. (2) will be 1.0 and there will be no change in the value of $(C_{\ell_P})_{\mathrm{TM}}$.

A convenient way to model the nonlinear effects of dynamic pressure on the roll damping moment is to increase the 0-deg-AOA value of C_{ℓ_P}, in comparison with the pitch damping methodology of [31]. However in using the [31] methodology in conjunction with C_{ℓ_P} at $\alpha = 0$, one must keep in mind the fact that C_{ℓ_P} at $\alpha = 0$ assumes that all four fins are effective, whereas at AOA, the leeward plane fins become increasingly ineffective. Furthermore, at low subsonic speeds, wing stall becomes a more important issue, in some cases, actually decreasing the magnitude of C_{ℓ_P} as the AOA approaches stall. Hence, a model to modify the [31] methodology as AOA increases and Mach number decreases is needed. An approximate model that focuses on the compressibility and separation physical phenomena discussed earlier is given by

$$C_{\ell_P} = (C_{\ell_P})_{\alpha=0}\left\{0.3\left[\left(\frac{Q_L}{Q_\infty}\right) - 1\right]\left(\frac{b}{d_{\mathrm{ref}}}\right)^{3/4} - 0.2M_N + 1\right\} \quad (3)$$

$(C_{\ell_P})_{\alpha=0}$ of Eq. (3) is the improved value of roll damping moment discussed in [7]. Q_L/Q_∞ of Eq. (3) is derived in [31], except we now omit the term V_∞/V_L from the equation so that

$$Q_L/Q_\infty = \left[\frac{1 + [(\gamma-1)/2]M_\infty^2\cos^2\alpha}{1 + [(\gamma-1)/2]M_\infty^2}\right][1 + \gamma M_\infty^2 \sin^2\alpha] \quad (4)$$

Equation (4) is plotted in Fig. 3 for convenience. Note that V_∞/V_L was omitted from the [31] approach because there was no oscillation motion involved in the roll damping motion derivation, unlike pitch damping. M_N of Eq. (3) is the Mach number normal to the body, $M_\infty \sin\alpha$.

Some explanation is in order for the derivation of Eq. (3). Referring to Fig. 2, Eq. (3) attempts to address the physical phenomena of increases in roll damping due to compressibility in the windward plane [the first term inside the outer bracket of Eq. (3)] and the loss of the effectiveness of the leeward plane fins due to being in the low-pressure region [the second term inside the outer bracket of Eq. (3)]. Of course, if the AOA is zero, both the first and second terms of Eq. (3) are zero and Eq. (3) reverts back to the 0-deg-AOA value of roll damping. In Fig. 2, notice the effect on each fin in roll as the AOA increases. As the AOA increases, those fins heading in the direction of increased dynamic pressure become more effective in roll damping (fins 1 and 2), whereas those fins heading into a region of lower dynamic pressure (fins 3 and 4) become less effective in roll damping. Equation (3) assumes that fins 1 and 3 cancel each other out, whereas fin 2 increases roll damping and fin 4 decreases roll damping. Actually, Eq. (3) allows for 30% of the windward plane to increase and 20% of the leeward plane to decrease roll damping, with the other 50% of the fins cancelling each other out. Initially, a value of 0.25 was assigned to both the windward and leeward plane fins, but in comparison with the data, the 0.3/0.2 split appeared to be a better fit. Also, the term $(b/d_{\mathrm{ref}})^{3/4}$ recognizes the fact that longer span fins are more effective than shorter span fins at producing roll damping. Also note that Eq. (3) does not account directly for the wing C_{N_α} and wing-stall physics of Fig. 2. Finally, if the fins are located on a flare, the effective AOA used in Eq. (4) and Fig. 3 is $\alpha + \theta_f$, where θ_f is the flare angle. Thus, a fin located on a flare will be in a region of higher dynamic pressure. The effect of fins on a boat tail was accounted for in the improved 0-deg-AOA value of C_{ℓ_P} discussed in [7]. Equation (3) will be referred to as method 1 for nonlinear roll damping predictions.

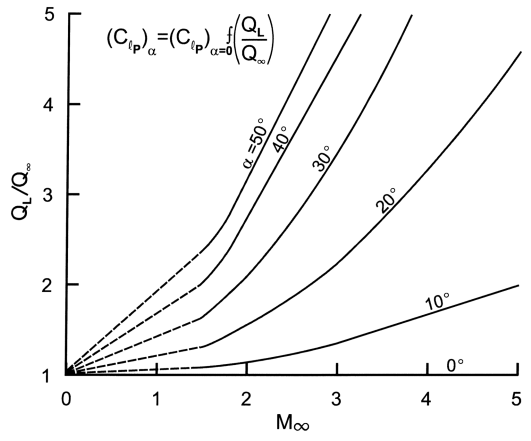

Fig. 3 Approximate relationship to allow roll damping nonlinearities to be estimated based on C_{ℓ_P} at a 0-deg AOA.

A second method to predict nonlinear roll damping used the idea of Eastman [29] [Eq. (1)], but extends Eastman's approach in the nonlinear AOA range. Initially, Eq. (1) was tried directly, where C_{ℓ_δ} was computed using the nonlinear values of C_{ℓ_δ} using the fourth-order wing-alone solution in the Aeroprediction code (see [5], pp. 200–208). Using the Eastman [29] approach directly met with some success, but overpredicted roll damping significantly for configurations with long boat tails, in comparison with the AP05. An approach that appears to offer more promise, however, is given by

$$C_{\ell_P} = (C_{\ell_P})_{\alpha=0} + 4.3[(C_{N_\delta})_{\alpha=0} - (C_{N_\delta})_\alpha]\left(\frac{\bar{y}}{d_{\mathrm{ref}}}\right)^2(\mathrm{MFF})f(\alpha) \quad (5)$$

where

$$f(\alpha) = 1 - \frac{.02|\alpha - \theta_f|}{(\bar{y}/d_{\mathrm{ref}})} \qquad f(\alpha) \geq 0.5$$

Equation (5) uses the 0-deg-AOA value of roll damping based on the improvements in roll damping discussed in [7] and uses the Eastman [29] approach to compute the change in roll damping due to AOA and nonlinear effects from stall. In particular, Eq. (5) addresses the physical phenomena of nonlinear wing lift with aspect ratio and AOA (and, to some extent, stall of Fig. 2) by using the nonlinear wing-alone lift methodology of [5]. The multifin factor (MFF) of Eq. (5) is the multifin factor of [7] and $f(\alpha)$ is the viscous effects of boundary-layer separation in the leeward plane. Notice that $f(\alpha)$ is allowed to decrease the nonlinear term of roll damping by as much as 50%.

The question naturally arises as to whether methods 1 or 2 are superior to one another or if each method is superior in a given region. Figure 4 addresses this question. In using methods 1 and 2, it was found that method 1 was superior for higher-aspect-ratio configurations ($AR \geq 1.0$) in which the normal Mach number was greater than about 0.6. This would imply that the physical phenomena of compressibility and viscous separation in the leeward plane were the dominant physics involved for this class of configurations and freestream conditions. On the other hand, it was found that method 2 was superior to method 1 for low values of normal Mach ($M_N \leq 0.2$) numbers or aspect ratio ($AR \leq 0.5$). The implication here is that for this class of configurations and freestream conditions, wing nonlinear lift-curve slope and viscous effects are the dominant physics involved. It was found that for regions between those in which methods 1 and 2 were best, a blend of methods 1 and 2 worked well. Referring to Fig. 4, in region 3, we have

$$C_{\ell_P} = (1) + \left(\frac{1 - AR}{0.5}\right)((2) - (1)) \quad (6a)$$

where (1) and (2) refer to methods 1 and 2, respectively. Likewise, for region 4 of Fig. 4, we have

$$C_{\ell_P} = (1) + \left(\frac{0.6 - M_N}{.40}\right)((2) - (1)) \quad (6b)$$

AP09 Nonlinear Roll Damping Model

① Compressibility and separation major phenomena

$$C_{\ell_P} = \left(C_{\ell_P}\right)_{\alpha=0}\left\{0.3\left[\left(\frac{Q_L}{Q_\infty}\right)-1\right]\left(\frac{b}{d_{ref}}\right)^{3/4} - 0.2\,M_N + 1\right\};\ M_N \geq 0.61$$

$$AR \geq 1.0$$

② Wing C_{N_δ} and viscous effects major phenomena

$$C_{\ell_P} = \left(C_{\ell_P}\right)_{\alpha=0} + 4.3\left[\left(C_{N_\delta}\right)_{\alpha=0} - \left(C_{N_\delta}\right)_\alpha\right]\left(\frac{\bar{y}}{d_{ref}}\right)^2 (MFF)\,f(\alpha);\ M_N \leq 0.2$$

$$AR \leq 0.5$$

Where: $f(\alpha)=1-0.02\,[|\alpha-\theta_f|/(\bar{y}/d_{ref})]$; $f(\alpha)\geq 0.5$

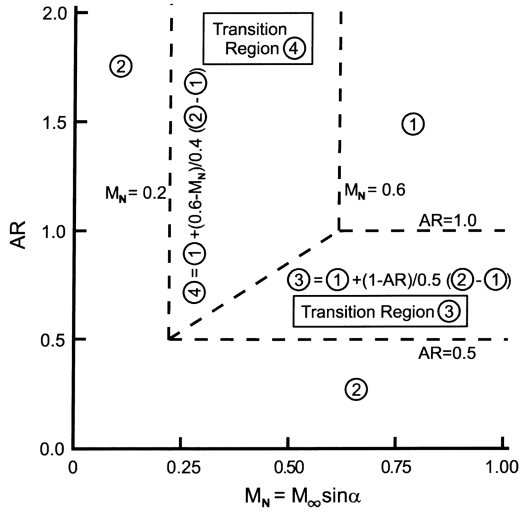

Fig. 4 Area of applicability of methods 1 and 2 to predict roll damping as a function of aspect ratio and normal Mach number.

Equations (6a) and (6b) imply that all the physical phenomena of Figs. 1 and 2 are important in the transition regions (3) and (4) of Fig. 4.

Suffice it to say that Fig. 4 and Eqs. (2), (3), (5), and (6) were derived based on a meager amount of experimental data. It is believed that the present semi-empirical method to predict nonlinear roll damping on wing–body–tail configurations is a good first cut. However, as more data become available, Fig. 4 and Eqs. (3), (5), and (6) could be revised.

Results and Discussion

Several data sets are available to compare with the new semi-empirical roll damping model of Fig. 4 for accuracy and robustness. The first case considered is the ANF configuration. Comparison of the new theory with available experimental data [8,11,15] is shown in Fig. 5 for $M_\infty = 4.1$, 2.54, and 0.22. Two sets of data are available for the $M_\infty = 0.22$ and 2.54 cases. One set of data is from the Arnold Engineering Development Center [8,15] and the other data set is from the former Naval Ordnance Laboratory [11] (now part of the Arnold Engineering Development Center). At $M_\infty = 4.1$, the new theory does an excellent job of following the data up to AOA 20 deg. At $M_\infty = 2.54$, the AP09 does a good job of following the trends of the data and is much more accurate than the AP05. At $M_\infty = 0.22$, the AP09 has the correct trend at both low and high AOA but overpredicts the loss of damping as AOA increases. The poor agreement of theory and experiment at $M_\infty = 0.22$ above $\alpha =$ 15 deg is probably due to not accounting for nonlinearities in roll moment due to roll rate or asymmetric shedding of the body vortices. Referring back to Fig. 4 and using the $M_\infty = 2.54$ case as an example, Eq. (5) is used up to AOA of about 5 deg, Eq. (3) is used for AOA above 14 deg, and both Eqs. (3) and (5) are blended together for AOA in between 5 and 14 deg.

The second case considered is the modified finner, for which a more extensive database [8,15] exists. The configuration and results of comparison of the AP05 and AP09 theories with experiment are shown in Fig. 6. Results are shown for $M_\infty = 0.6$, 0.9, 1.3, 1.5, 2.0, 2.25, and 2.5 up to $\alpha = 40$ deg. In all cases, the AP09 gives the correct initial trend of the data, and at $M_\infty = 1.5$, 2.0, 2.25, and 2.5, it compares very well to the data. At $M_\infty = 0.6$, the new theory compares well to experiment up to AOA 15 deg but does not predict the sharp drop-off in roll damping at $\alpha = 20$ deg. At $M_\infty = 0.9$, the AP09 overpredicts the maximum value of C_{ℓ_p} at AOA 10 to 15 deg but predicts the C_{ℓ_p} values at high AOA quite well. Again, the poor agreement at $M_\infty = 0.6$ and $\alpha > 15$ deg may be due to the neglect of nonlinearities due to high roll rate or asymmetric shedding of the body vortices. At $M_\infty = 1.3$, predictions are excellent up to $\alpha = 20$ deg, where a sharp increase in C_{ℓ_p} data is noted at $\alpha =$ 25 deg and higher. It is not clear what causes this sharp increase in C_{ℓ_p}, but wind-tunnel-wall interference of the shock onto the tail is a possibility. In general, the AP09 nonlinear method is clearly superior to the linear AP05 roll damping methodology for the Fig. 6 configuration.

The next three cases are for the MK 82 low-drag bomb and two candidate replacements for the MK 82 bomb, referred to as the fixed

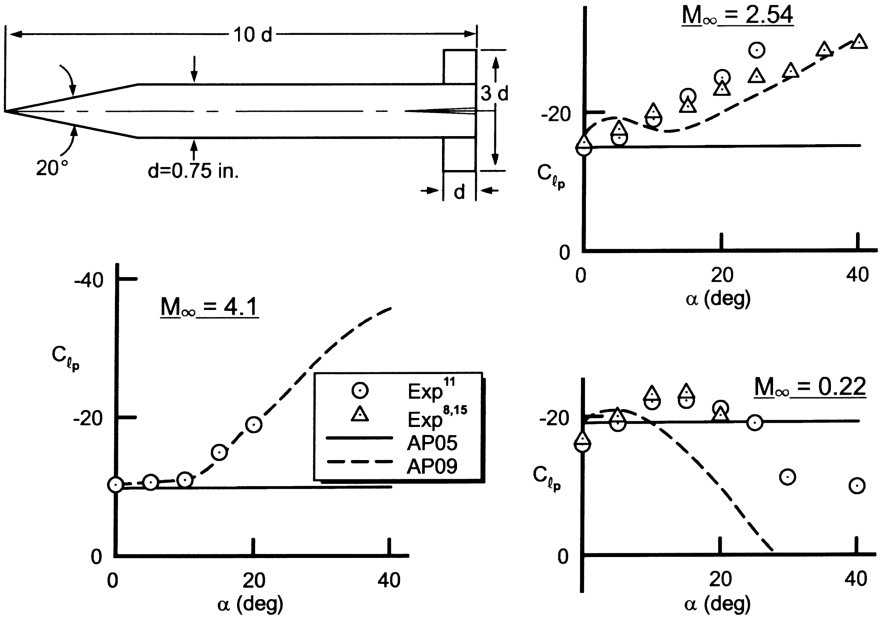

Fig. 5 Comparison of theory and experiment for roll damping of the ANF.

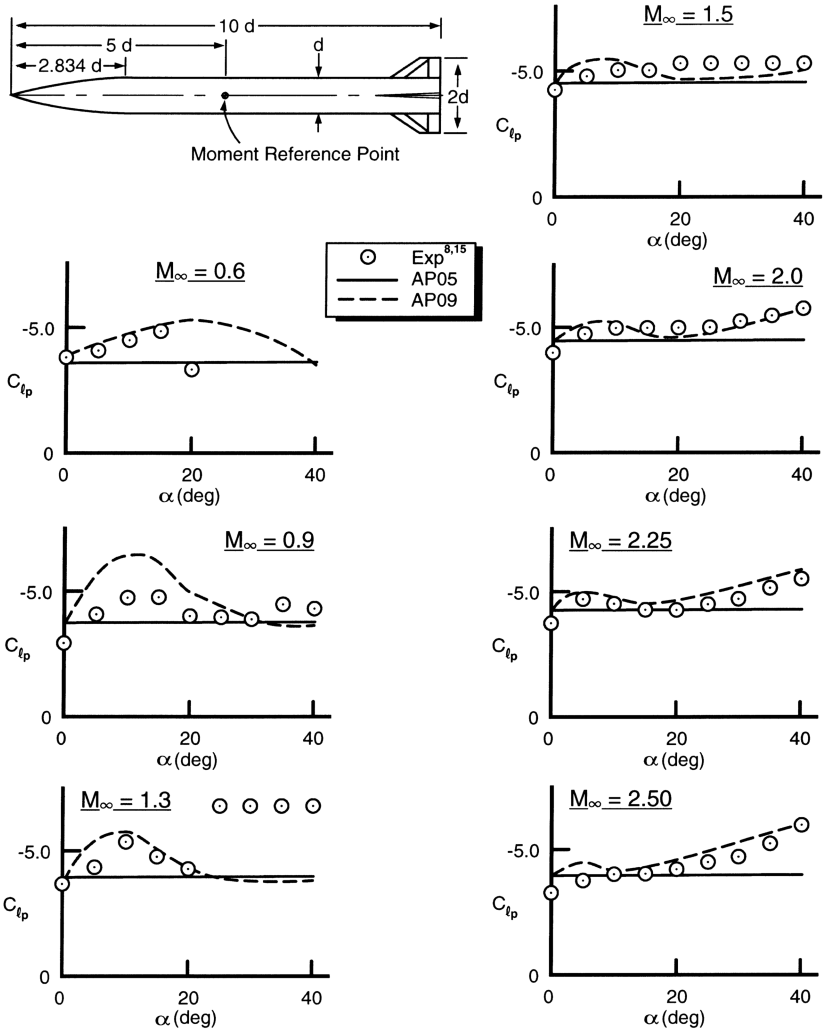

Fig. 6 Comparison of theory and experiment for roll damping of the MANF.

fin (FF) and an inflatable stabilizer/retarder extended (ISRE). Figure 7 compares the AP05 and AP09 predictions with roll damping experimental data [10] at $M_\infty = 0.8$ for AOA up to 30 deg for the MK 82 low-drag bomb. In general, the AP09 follows the data trends and compares quite well with the data, except at $\alpha = 25$ deg and higher, where the theory gives too low a value of roll damping. Again, the AP09 nonlinear theory is clearly superior to the linear AP05 methodology.

Figure 8 shows the comparison of the AP05 and AP09 roll damping predictions with the experiment for the MK 82 candidate FF configuration at $M_\infty = 0.8$, 1.0, and 1.2 up to AOA of 25 deg. In examining Fig. 8, it is seen the AP09 again does a good job of following the trends of the experimental data. The AP09 predictions are slightly high for AOA greater than 10 deg but are clearly superior to the AP05 predictions, except at $\alpha = 0$ deg.

Figure 9 gives results for the ISRE roll damping predictions compared with the experiment. The ISRE is an 8-fin configuration with a flare and the fins are located on the flare. C_{ℓ_P} predictions of the AP09 and AP05 are again compared with the experiment at $M_\infty = 0.8$, 1.0, and 1.2 at AOA up to 25 deg. Here, the AP09 shows significant improvement over the AP05 in roll damping predictions, even at a 0-deg AOA. The reason for the AP09 improvement in roll damping prediction over the AP05 at a 0-deg AOA is the fact that the AP09 accounts for the flare in the Fig. 4 methodology, whereas the AP05 does not.

The next case considered is the 81-mm mortar configuration shown in Fig. 10. Comparison of theory and experiment up to 10 deg AOA at $M_\infty = 0.5$ and 0.8 is shown in the figure. The data suggest a slight nonlinearity in C_{ℓ_P} with increasing AOA, but not as large as

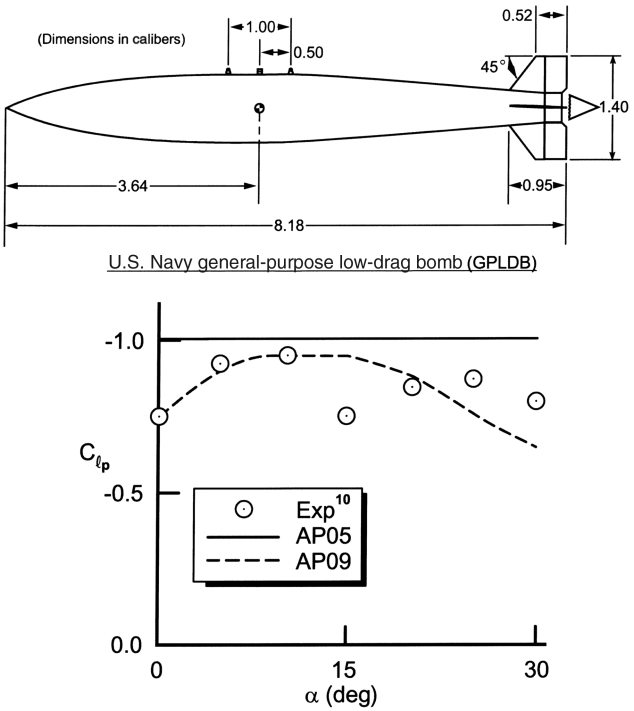

Fig. 7 Comparison of theory and experiment for roll damping of the MK 82 low-drag bomb ($M_\infty = 0.8$).

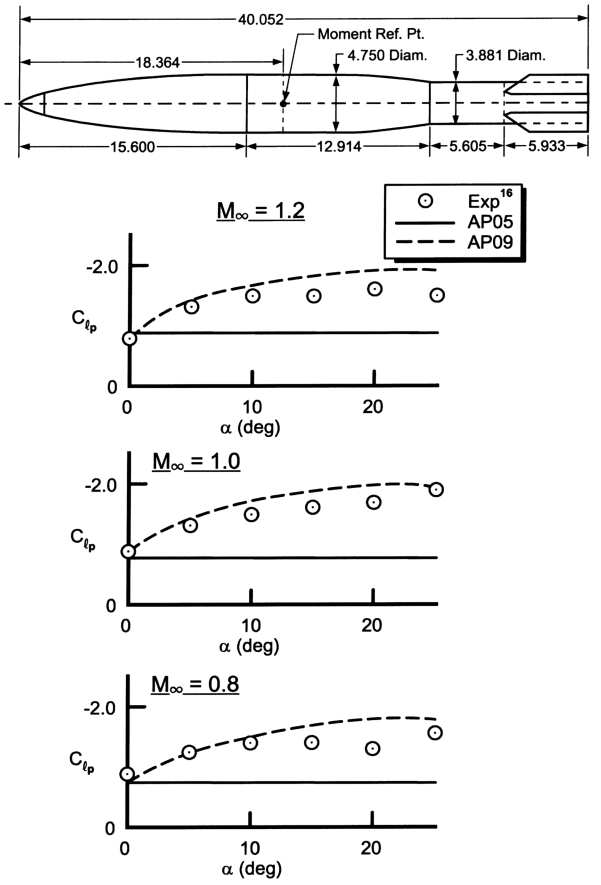

Fig. 8 Comparison of theory and experiment for roll damping of the FF candidate for the MK 82 store.

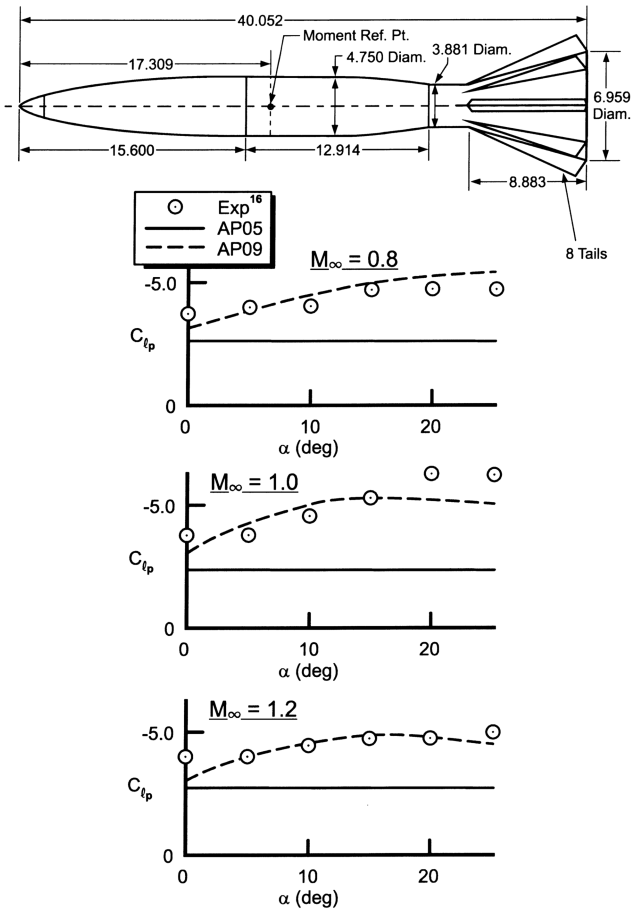

Fig. 9 Comparison of theory and experiment for roll damping of the ISRE candidate for the MK 82 store.

predicted by the AP09. Even so, the AP09 roll damping predictions are still superior to those of the AP05.

The next two cases illustrate the capability of the AP09 to predict roll damping of configurations that have two sets of lifting surfaces. The first case is a canard-controlled missile configuration shown in Fig. 11. Wind-tunnel tests [17,18] were conducted in a component buildup fashion that allows comparison of the AP05 and AP09 to body–canard, body–tail, and canard–body–tail configurations. Results are shown in Fig. 11 at $M_\infty = 0.1$ for $\alpha = 0$–30 deg. In general, the comparison of the AP09 predictions to experiment is quite encouraging for all three configurations and is also superior to the AP05. Note the different trend of the body–tail data and body–canard data. The body–tail has a slight uptrend with α, due to a moderate aspect ratio (1.33), whereas the body canard has a decreasing trend with α, due to a large aspect ratio (3.53). The higher-aspect-ratio wings stall and therefore lower the lift-curve slope, causing the decrease in roll damping capability. It is noteworthy that the roll damping of the canard–body–tail is much lower than the addition of the canard–body and body–tail cases added together. This lower value of C_{ℓ_p} for the complete configuration is due to the loss of roll damping effectiveness of the tails from the canard-shed vortices. Note that the canard-shed vortex effects are reduced considerably at $\alpha = 25$ deg, because the vortices have mostly passed over the tails. On the other hand, at $\alpha = 30$ deg, another complexity has apparently affected the roll damping: the asymmetric shedding of vortices. Note the large difference in roll damping moment on the canard–body–tail case at $\alpha = 30$ deg between two different wind-tunnel tests of the same model in the same wind tunnel. Also note the sudden increase in C_{ℓ_p} for the body–tail case at $\alpha = 30$ deg. The implication of this figure is that for subsonic speeds, the new nonlinear methodology of the AP09 is questionable above $\alpha = 25$ deg, where asymmetric vortex shedding plays a role in the nonlinear aerodynamics.

The second canard–body–tail case is shown in Fig. 12. The Fig. 12 configuration has large wings and is quite similar in shape to a

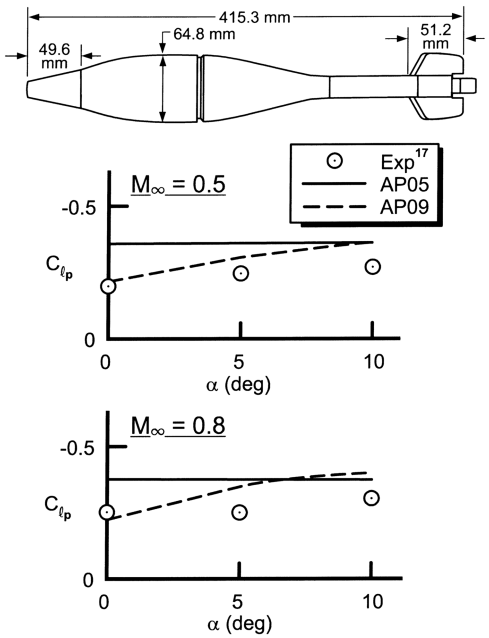

Fig. 10 Comparison of theory and experiment for roll damping of the 81-mm mortar.

Seasparrow missile. According to the AP09 C_{ℓ_p} predictions, the tail surface loses all roll damping effectiveness at a 0-deg AOA. This also agrees with the flight-test results [27] and clearly shows the AP09 predictions to be superior to the AP05.

In reviewing the results of the AP09 and AP05 when compared with the various configurations illustrated in Figs. 5–12, it is clear the

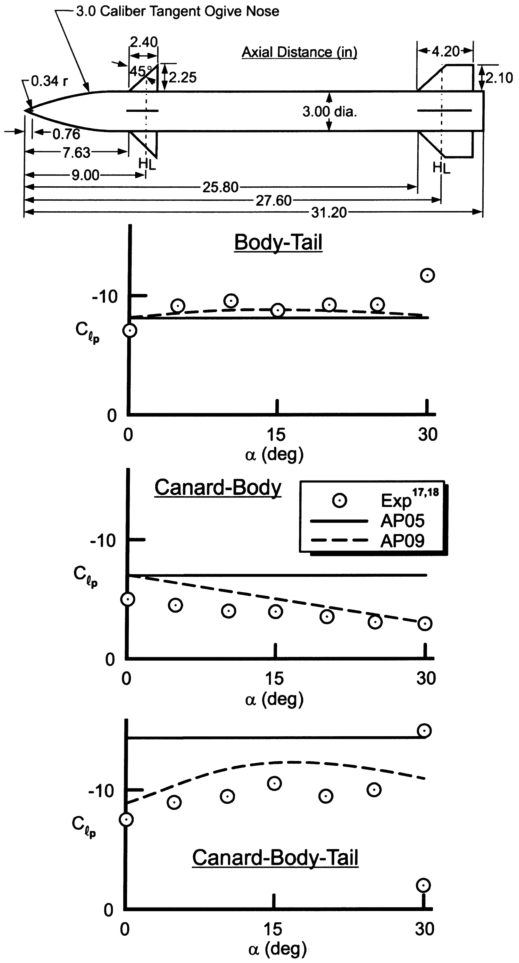

Fig. 11 Comparison of theory and experiment for roll damping for the canard-control missile configuration ($M_\infty = 0.1$).

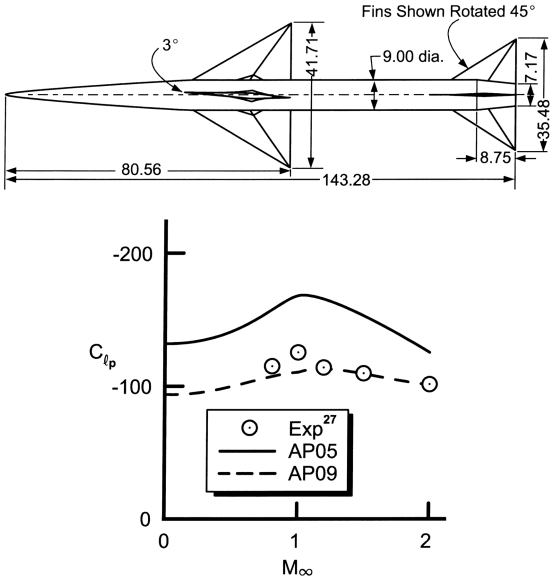

Fig. 12 Comparison of theory and flight tests for roll damping of the wing–body–tail case at $\alpha \approx 0$.

Fig. 4 methodology for nonlinear roll damping correctly captures most of the physics involved in the increases or decreases in roll damping as AOA increases. It is also shown that the AP09 is clearly superior to the AP05, which has no nonlinear roll damping prediction capability. The AP09 also appears to be fairly robust in the roll damping predictions in that configurations with boat tails, flares, four to eight fins, and one and two sets of lifting surfaces, Mach numbers of 0.1–4.1 and AOA to 40 deg were considered with reasonable accuracy at most conditions. The AP09 methodology of Fig. 4 can also be refined as more data become available.

Conclusions

To summarize, a new semi-empirical method was developed to predict the nonlinear roll damping moment on wing–body–tail configurations. The new methodology attempts to account for the physical phenomena that cause the roll damping nonlinearities, including wing lift-curve slope, wing-stall effects, dynamic pressure effects at angle of attack, canard-shed vortices, and fins located on a flare or boat tail. The method does not account for the physical phenomena of nonlinear rolling moment due to high spin rate or asymmetric shedding of the body vortices. Both nonlinearities due to spin rate and asymmetric vortices appear to be significant at Mach numbers below 1.5 and angles of attack greater than about 20 deg. Comparison of the new method to a limited amount of experimental data on a range of configurations and flight conditions showed encouraging results. However, additional data combined with more accurate computational fluid dynamics computations on additional configurations would allow refinement of the new method.

References

[1] Moore, F. G., and Swanson, R. G., Jr., "Aerodynamics of Tactical Weapons to Mach Number 3 and Angle of Attack 15° Part 1: Theory and Application," Naval Surface Weapons Center TR-3584, Dalhgren, VA, Feb. 1977.

[2] Martin, J. C., and Jeffreys, I., "Span Load Distribution Resulting from Angle-of-Attack, Rolling, and Pitching for Tapered Sweptback Wings with Streamwise Tips," NACA TN 2643, 1952.

[3] Malvestuto, F. S., Jr., Margolis, K., and Ribner, H., "Theoretical Lift and Damping in Roll at Supersonic Speeds of Thin Sweptback Tapered Wings with Streamwise Tips, Subsonic Leading Edges, and Supersonic Trailing Edges," NACA TR 9780, 1950.

[4] Chadwick, W. R., "The Application of Non-Planar Lifting Surface Theory to the Calculation of External Store Loads," *AIAA Journal*, Vol. 11, Mar. 1974, pp. 181–188.

[5] Moore, F. G., *Approximate Methods for Weapon Aerodynamics*, AIAA Progress in Astronautics and Aeronautics, Vol. 186, AIAA, Reston, VA, Aug. 2000.

[6] Whyte, R. H., "SPINNER—A Computer Program for Predicting the Aerodynamic Coefficients of Spin Stabilized Projectiles," General Electric Co., Class 2 Reports, 1969.

[7] Moore, F. G., and Moore, L. Y., "Improved Aerodynamics for Configurations with Boat Tails," *Journal of Spacecraft and Rockets*, Vol. 45, No. 2, Mar.–Apr. 2008, pp. 270–281. doi:10.2514/1.29687

[8] Uselton, B. L., and Jenke, L. M., "Experimental Missile Pitch and Roll Damping Characteristics at Large Angles of Attack," *Journal of Spacecraft and Rockets*, Vol. 14, No. 4, Apr. 1977, pp. 241–247.

[9] Pierens, D. A., "Pitch and Roll Damping Coefficients of the Australian 81 mm Improved Mortar Projectile," Defense Systems and Technology Operation TR-0020, Washington, D.C., May 1994.

[10] Piper, W. D., and DeMeritte, F. J., "Summary of the NOL Investigations to Date of the Aerodynamic Characteristics of the Navy Low Drag Bomb," U.S. Naval Ordnance Systems Command Rept. 5679, Washington, D.C., Feb. 1960.

[11] Regan, F. J., "Roll Damping Measurements for the Basic Finner at Subsonic and Supersonic Speeds," U.S. Naval Ordnance Systems Command Rept. 6652, Washington, D.C., Mar. 1964.

[12] Vlajurae, M., "Wind Tunnel Measurements of the Aerodynamic Characteristics of the 2.75 Wrap Around Fin Rocket Using a Magnetic Suspension System," Aerophysics Lab., Massachusetts Inst. of Technology TR 150, Cambridge, MA, Dec. 1968.

[13] Owens, S., Dohren, R., and Malihke, G., "High Speed Wind Tunnel Test, Precision Guided Mortar Munition (PGMM)," Test Rept. 101, EMHSWT 1419, ATK Missile Systems Co., Rocket Center, WV, Apr. 2005.

[14] Owens, S., Dohren, R., Sitts, J., and Malejko, G., "Precision Guided Mortar Munition (PGMM)," Test Rept. 101B, Pt. 2, Tank-Automotive and Armaments Command, Armament Research Development and Engineering Center, Picatinny Arsenal, NJ.

[15] Jenke, L., "Experimental Roll-Damping, Magnus, and Static Stability

Characteristics of Two Slender Missile Configurations at High Angles of Attack (0 to 90 Deg) and Mach Numbers 0.2 through 2.5," Arnold Engineering Development Center TR-76-58, Tullahoma, TN, July 1976

[16] Wallace, A. R., and Shadow, T. O., "Magnus and Roll Damping Characteristics of the Fixed-Fin and Inflatable Stabilizer Retarder Configuration of the MK 82 Store at Transonic Speeds," Arnold Engineering Development Center TR-75-163, Tullahoma, TN, May 1975.

[17] Hardy, S. R., "Nonlinear Rolling Motion Analysis of a Canard Controlled Missile Configuration at Angles of Attack from 0 to 30° in Incompressible Flow," Naval Surface Weapons Center TR-3808, Dalhgren, VA, May 1978.

[18] Hardy, S. R., "Subsonic Wind Tunnel Tests of a Canard-Control Missile in Pure Rolling Motion," Naval Surface Weapons Center TR-3615, Dalhgren, VA, June 1977.

[19] Uselton, J. C., and Carmen, J. B., "Wind Tunnel Investigation of the Roll Characteristics of the Improved 2.75 Inch-Diameter Folding Fin Aircraft Rocket at Mach Numbers from 2.5 to 4.5," Arnold Engineering Development Center TR-69-207, Tullahoma, TN, Nov. 1969.

[20] Carmen, J. B., Uselton, B. L., and Burt, G. E., "Roll Damping, Static Stability, and Damping-in-Pitch Characteristics of Axisymmetric Bomblet Munition Models at Supersonic Mach Numbers," Arnold Engineering Development Center TR-71-88, Tullahoma, TN, Apr. 1971.

[21] Shadow, T. O., "Transonic Roll-Damping and Magnus Characteristics of Three Bomblet Munition Models used in the Evaluation of Aerodynamic Dispersion Techniques," Arnold Engineering Development Center TR-71-33, Tullahoma, TN, Mar. 1971.

[22] Daniels, P., and Hardy, S. R., "Theoretical and Experimental Methods in the Solution of Missile Nonlinear Roll Problems," Naval Surface Weapons Center DL-TR-3773, Dahlgren, VA, Jan. 1978.

[23] Oberkampf, W. L., "Theoretical Prediction of Roll Moments on Finned Bodies in Supersonic Flow," 12th Aerospace Sciences Meeting, Washington, D.C., AIAA Paper 74-111, 1974.

[24] Oberkampf, W. L., "Prediction of Forces and Moments on Finned Missiles at High Angles of Attack in Transonic Flow," U.S. Air Force Advanced Technology Lab. TR-80-107, Austin, TX, Oct. 1980.

[25] Fuchs, H., "Prediction of Dynamic Derivatives," *Stability and Control of Tactical Missile Systems*, AGARD-CP-451, AGARD, Neuilly-sur-Seine, France, May 1988, Paper 6.

[26] Nicolaides, J. D., and Bolz, R. E., "On the Pure Rolling Motion of Winged and/or Finned Missiles in Varying Supersonic Flight," *JAS Journal*, Mar. 1953, pp. 160–168.

[27] Hopko, R. N., "A Flight Investigation of the Damping in Roll and rolling Effectiveness Including Aeroelastic Effects of Rocket-Propelled Missiles Having Cruciform, Triangular, Interdigitated Wings and Tails," NACA RM L51D16, Sept. 1951.

[28] Prakash, S., and Khurana, D. D., "A Simple Estimation Procedure of Roll-Rate Derivatives for Finned Vehicles," *Journal of Spacecraft and Rockets*, Vol. 21, No. 3, May–June 1984, pp. 318–320. doi:10.2514/3.25656

[29] Eastman, D. W., "Roll Damping of Cruciform Tailed Missiles," *Journal of Spacecraft and Rockets*, Vol. 23, No. 1, Jan.–Feb. 1986, pp. 119–120. doi:10.2514/3.25794

[30] Mikhail, A. G., "Roll Damping for Finned Projectiles Including: Wraparound, Offset and Arbitrary Number of Fins," U.S. Army Research Lab., TR-846, Aberdeen Proving Ground, MD, Aug. 1995.

[31] Moore, F. G., and Moore, L. Y., "New Methods to Predict Nonlinear Pitch Damping Moments," *Journal of Spacecraft and Rockets*, Vol. 45, No. 3, May–June 2008, pp. 495–503.

M. Miller
Associate Editor